THE JOURNAL OF PHYSICAL CHEMISTRY A
A JOURNAL OF THE AMERICAN CHEMICAL SOCIETY

pubs.acs.org/JPCA

Article

Very Low-Frequency Broadband Electron Paramagnetic Resonance Spectroscopy of Metalloproteins

Wilfred R. Hagen*

Cite This: *J. Phys. Chem. A* 2021, 125, 3208−3218

Read Online

ACCESS | Metrics & More | Article Recommendations | Supporting Information

ABSTRACT: A previously developed spectrometer for broadband electron paramagnetic resonance (EPR) spectroscopy of dilute randomly oriented systems has been considerably modified to extend the frequency reach down to the hundred MHz range and to boost concentration sensitivity by 1 to 2 orders of magnitude. The instrument is now suitable for the study of biological systems in particular metalloproteins. As a proof of concept, examples from the class of low-spin ferric hemoproteins are studied in terms of frequency-dependent changes in their EPR spectra. Mono-heme cytochrome *c* EPR is determined by g-strain over a wide frequency range, whereas a combination of unresolved ligand hyperfine interaction and concentration-dependent intermolecular dipolar interaction becomes dominant at very low frequencies. In the four heme containing cytochrome c_3, g-strain combines with intramolecular dipolar interaction over the full-studied frequency range of 0.23−12.0 GHz. It is concluded that the point-dipole approach is inappropriate to describe magnetic interactions between low-spin ferric heme systems and that a body of literature on redox interactions in multi-heme proteins will be affected by this conclusion.

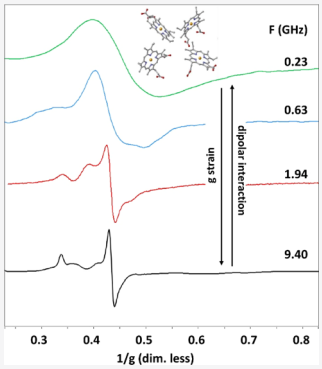

INTRODUCTION

The spin Hamiltonian of transition-ion complexes generally uses terms linear in the microwave frequency and terms independent of the frequency. Therefore, unequivocal spectral analysis requires data collection at multiple frequencies. To achieve this goal, I have recently described the development of a broadband spectrometer in which the conventional monochromatic cavity was replaced with a wire microstrip resonator circuit tunable over a wide range of frequencies. Proof of principle was shown in the case of 0.5% triclinic Cu(II) substitutionally added to $ZnSO_4$ with a data set collected from circa 0.8 to 12 GHz.[1] In a subsequent study to explore applicability to metalloproteins, in particular low-spin ferric hemoproteins, I encountered two practical limitations. First, although the broadband spectrometer had an excellent resolution, its concentration sensitivity was intrinsically low and only allowed for data collection by extensive averaging on hemoproteins prepared at the very high end of their solubility. Second, the study suggested that data taken at very low frequencies, 100−500 MHz, could be particularly interesting for the study of dipolar interaction in multi-center metalloproteins; however, with the inherently unfavorable Boltzmann distribution over the spin sublevels, concentration sensitivity became unpractically low. Furthermore, with lower microwave frequency, the remnant field of the electromagnet increasingly interferes with the desired spectroscopy.

Here, I describe several significant changes to the broadband detection design which make the spectroscopy practical for very low-frequency studies of dilute metal complexes. Concentration sensitivity is boosted by 1 to 2 orders of magnitude by adding conventional 100 kHz field modulation to the signal detection, which, however, dictates that the direct detection by the vector signal transceiver (VST) is replaced with detection by broadband RF detection diodes. An additional gain in sensitivity is obtained at low microwave frequencies by replacement of the slowly scanning electromagnet with a scanning multiple set of Helmholtz coils to raise the field scan rate from at least 20 s to 10 ms per single scan. The resonator circuitry is also modified to include a very long optical path of 20−60 m to create many sharp loaded-Q resonances or "dips". The spectrometer is extensively tested, and dedicated software is developed for its control and for data analysis. Applicability is illustrated on the class of low-spin hemoproteins by comparison of broadband data from a mono-heme versus a tetra-heme cytochrome. Spectral broadening contributions from superhyperfine (SHF) interaction and dipolar interaction are disentangled. The latter is found to be more prominent than predicted by the point-dipole model and to interfere with redox-interaction analysis from conventional X-band data.

EXPERIMENTAL SECTION

The spectrometer is described in general terms, below, in the Results and Discussion section. A complete list of parts is given in Supporting Information, section spectrometer hardware

Received: February 9, 2021
Revised: March 29, 2021
Published: April 13, 2021

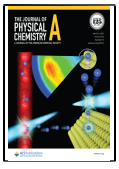

https://doi.org/10.1021/acs.jpca.1c01217
J. Phys. Chem. A 2021, 125, 3208−3218

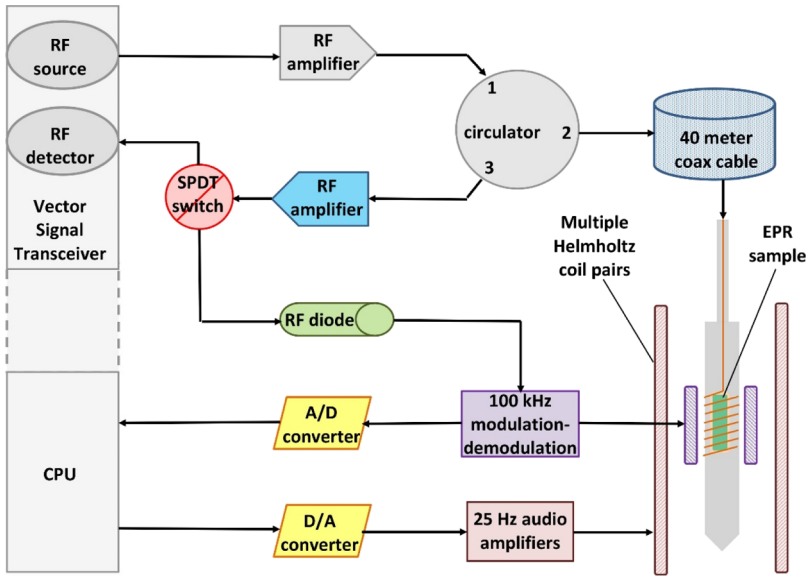

Figure 1. Schematic overview of the broadband spectrometer's low-frequency version. Previously described parts are shown in gray; newly added elements are shown in color. The RF source produces a microwave of 65 to circa 700 MHz, which is sent via a circulator into a resonator circuit consisting of an elongation cable and a wire microstrip cell in which some of the dielectric isolation is replaced with the paramagnetic sample.[1] The reflected RF part goes either to the monochromatic direct detector or is switched to an alternative branch for detection in a broadband RF diode and conversion to a video signal, which is demodulated in a 100 kHz field modulation unit and digitized for storage. The magnet consists of five Helmholtz pairs of coils driven by high-power audio amplifiers from a software generated sine wave at 25 Hz to produce a repeated field scan of circa 0−250 G in 10 ms. Note the extreme length of the coaxial elongation cable required to produce resonator dips of sufficient number and with a sufficiently high loaded-quality factor.

(Figure S1 and Tables S1 and S2). Software for the operation of the spectrometer and data manipulation and for a variety of spectral simulations was written in LabVIEW graphical language, using the LabVIEW professional development system 2020, with calls to dynamic link libraries for the computational-intensive procedures written in FORTRAN using the Intel Visual Fortran Compiler 2020 integrated into the Microsoft Visual Studio Community 2019 development environment. The simulation programs are described in Supporting Information, section software. The complete source code is provided in a separate zip file. Software for the simulation of multi-component spectra subject to g-strain has been described previously.[2] Horse heart cytochrome *c*, type C2506, was obtained from Sigma-Aldrich (Sigma-Aldrich Chemie N.V., Zwijndrecht, The Netherlands). Cytochrome c_3 from *Desulfovibrio vulgaris* (Hildenborough) was isolated and purified, as described previously.[3]

RESULTS AND DISCUSSION

General Spectrometer Design. The new spectrometer has two different magnets: a conventional electromagnet for measurements from circa 0.5 to 18 GHz and a rapid scanning coil assembly for measurements from 65 to circa 700 MHz. A schematic overview of the low-frequency version of the spectrometer setup is presented in Figure 1 with emphasis on those elements in which the present design differs in essence from the previous broadband machine.[1]

The new items are shown in color; those retained from the previous design are grayed. A complete description of all parts is given in Figure S1 and Tables S1 and S2. The most conspicuous change is the replacement of the slowly scanning electromagnet with a collection of Helmholtz coils driven at 25 Hz which produces a sinusoidal field between $\pm B_{max}$ whereby the complete field scan is ran four times every 40 ms, that is, each individual scan takes 10 ms. Compared with the typical scan rate of a few minutes in a conventional spectrometer this is a reduction in scan time by over 4 orders of magnitude and thus a potential gain in the signal-to-noise ratio of over 2 orders of magnitude for equal data collection time. The magnet coils are cooled with forced air by two blowers with a joint capacity of 220 L/s. Herewith, the temperature of the coil assembly is sufficiently stable to guarantee a B_{max} of 250 G which is reproducible within 0.2% (0.5 G) over 10,000 individual scans in 100 s. Better field stability, or more extensive data sets with the same field stability can be collected with short shutdown periods, typically a few seconds, of the coils in between 100 s runs. For $g = g_e$, a maximum field of 250 G corresponds to a microwave frequency of 700 MHz; however, due to the nonlinearly changing scan rate, resolution deteriorates at the high end of the field scan. The spectrometer is routinely run between 65 and circa 500 MHz.

The previously developed wire microstrip cell with the sample sandwiched between a metal ground plate and a thin coiling metal wire[1] is retained, and only the resonance structure, which runs from circulator port 2 till the open RF end of the cell, is changed in that the previous 'long' coax stretch of up to a few meters is now replaced with a very long cable of 20−60 m. This extreme optical path is required at low microwave frequencies to ensure that the organ-pipe effect of standing waves produces sufficient resonance dips with sufficiently high loaded *Q*-factor (Figure S2). On the other hand, the trombone-type RF phase shifter, used in the previous design to fine-tune these resonance dips, has now been removed as its internal maximum length has become negligibly small compared to the overall path.

In a reversion to conventional electron paramagnetic resonance (EPR) methodology, the present spectrometer also includes magnetic field modulation at 100 kHz as a means to further boost the signal-to-noise ratio by another 1 or 2 orders of

https://doi.org/10.1021/acs.jpca.1c01217
J. Phys. Chem. A 2021, 125, 3208−3218

magnitude. This, however, requires signal detection by means of an RF diode to transfer the RF signal into a video one for the demodulation unit. In turn, the diode characteristics demand that for maximal signal-to-noise ratio, the detected RF be of sufficient power, that is, of the order of 0−20 dBm, and in combination with the sharp-dip forming long path, this then requires an extra RF amplifier following port-3 of the circulator. By means of a single pole, double throw (SPDT) switch following the extra RF amplifier, the option to use the original route to direct detection by the VST is retained to allow for monitoring and optimization of the RF mode pattern. Also, the magnet and sample cell are dimensioned such that they can accommodate an existing simple helium-flow system[4] for low-temperature measurements.

The above scheme is also used for measurements above 500 MHz except that the coil assembly is replaced by a conventional electromagnet, and instead of the ≥20 m elongation cable, a broadband phase shifter is reinstated.

Data Collection Procedure. In a single period of sinusoidal variation of the magnetic field, the low-frequency EPR spectrum is scanned four times: positive up, positive down, negative down, and negative up. The scan is also non-linear in the field, so the four scans have to be combined into one and subsequently linearized (Figure 2).

The fourfold combining must be preceded by an overall field shift (i.e., by an element rotation of the digital spectral array) so that the spectrum starts at a phase equal to zero or to an integer multiple of $\pi/2$. The spectrum is subsequently split into two-halves that are folded (i.e., overlaid as mirror images), and the resulting twofold spectrum is split once more, and the first half is again overlaid with the mirror image of the second half which is now also subjected to a vertical sign change. In the case of direct detection, when the switch, as shown in Figure 1, is opened toward the VST, we measure the EPR absorption spectrum and all four sub-spectra have the same amplitude sign so that their correct overlay should maximize the signal amplitude. When, however, the field is additionally 100 kHz modulated, with the switch, as shown in Figure 1, opened toward the broadband RF diode detector, we observe the conventional first derivative EPR whose sign depends on the direction of the field scan. The sign variation is retained when we integrate the spectrum to make automated analysis more robust by minimizing baseline instabilities. With sinusoidal field variation, the signs of course come in a fixed order, for example + − − + when we start with a positive downfield scan (i.e., the phase of the sine wave is 90°) and in the overlay procedure, we must change the sign of the second half in the second mirroring operation. The whole procedure is illustrated in Figure 2 and can be symbolized as

$$(\text{new array})_1 = \max_n |\iota \times \sigma \times R_n(\text{array})_4| \quad (1)$$

in which $(\text{array})_4$ is the observed fourfold spectrum of dimensionality n, R_n is the digital rotation, or "bin shift", over n elements, σ is the mirroring (with respect to a vertical axis through the center of the spectrum) and addition of the two spectral halves, ι is the inversion, that is, the mirroring and negative addition of the new two-halves, max is the maximization of the absolute spectral amplitude as a function of n, and (new array) is the resulting fourfold averaged single EPR absorption scan of dimensionality $n/4$.

In conventional field-modulated EPR, the demodulation unit usually has a build-in low-pass noise filter in the form of a simple RC filter. Here, it must be disabled because its operation, in combination with rapid-field scanning, leads to integration of the derivative spectrum and also to broadening proportional to the time constant τ = RC even for τs in the microsecond range.

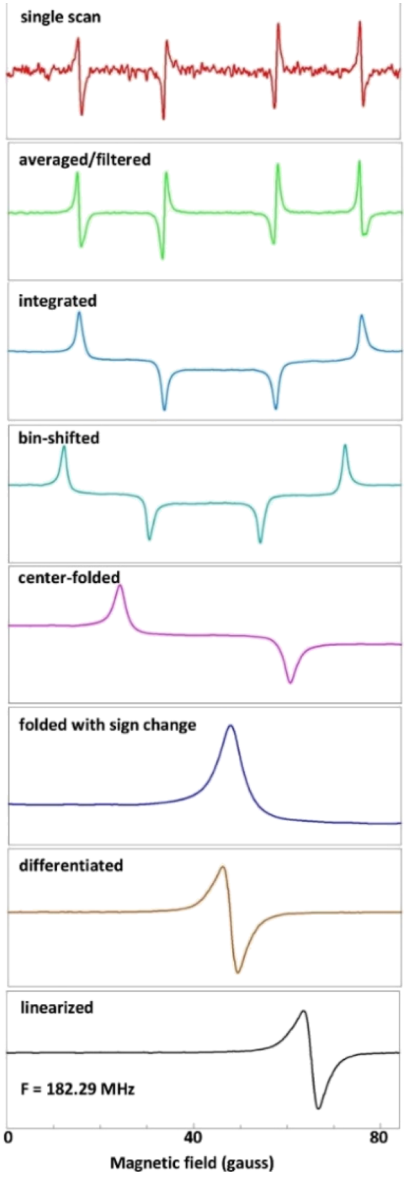

Figure 2. Data collection procedure with the multi-coil scanning magnet. A single period of the 25 Hz sinusoidal magnetic field affords four concatenated spectra in 40 ms. Following averaging, filtering, integration, and digital phase shifting (bin shifting), the four spectra are combined, differentiated, and the field scale is linearized. See the text for more details. This example is a 100× averaged fourfold spectrum of solid 2,2-diphenyl 1-picryl hydrazyl (DPPH) at 182.29 MHz and a dip power of +10 dBm.

In both detection schemes, direct versus field-modulated, the resulting spectrum is on a non-linear field scale defined by the 25 Hz sinusoidal variation in which dB/dt varies from its maximal value at zero field to zero-valued in the $\pm B_{max}$ turning points, where the sine phase is $\pi/2$ or $3\pi/2$ assuming that the transfer function between the digitally generated sine wave and the magnetic field is a perfect constant. To test this assumption, I measured the sharp, single-line spectrum of solid DPPH powder at 53 different frequencies in the range 66−719 MHz using four broadband circulators with adjacent frequency ranges.

https://doi.org/10.1021/acs.jpca.1c01217
J. Phys. Chem. A 2021, 125, 3208−3218

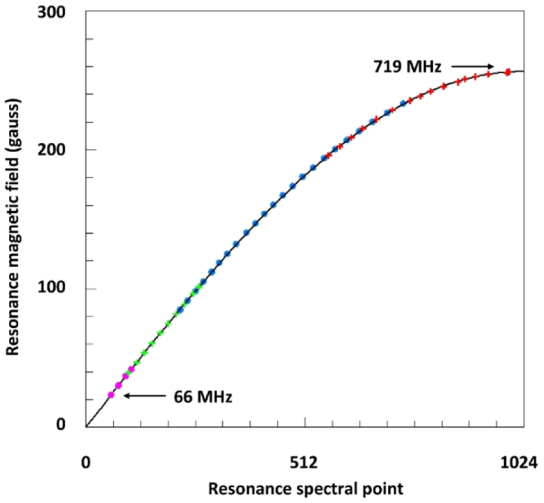

Figure 3. Testing of the sinusoidal rapid-field scan with DPPH at 53 frequencies. Data were collected with four different circulators: 66−88 MHz (magenta), 100−200 MHz (green), 225−400 MHz (blue), and 630−780 MHz (red). The elongation path was 40 m in all cases. The poor overlap between the circulators was compensated for by the high intensity of the DPPH signal. Each scan was averaged for 160−400 s except for the lowest-frequency ones (magenta), which took 1000 s. The resonance magnetic field (g = 2.0036) plotted as a function of the spectral point interpolated over 1024 bins perfectly coincided with the first quarter of a sine wave.

As shown in Figure 3, the resonance field B_{res} is plotted versus the x-axis digital position (i.e., bin number) of the resonance peak and is found to excellently fit the first quarter of a sine wave

$$B_{res} = B_{max} \times n \times \sin\left(\frac{x}{n} \times \frac{\pi}{2}\right) \quad (2)$$

confirming the assumption of constant transfer. B_{max} is the maximal field value of the Helmholtz coil assembly for a given amplitude setting (volts) of the digitally generated sine wave. Thus, data can be converted to a linear field scale by means of the transformation in eq 2.

Finally, the spectrum resulting from the direct detection scheme is numerically differentiated for ease of comparison with conventional EPR data. Usually, also a noise-reduction filter is applied within the limits of no loss of spectral resolution. In my standard procedure, a Savitzky−Golay filter of polynomial order 3 is applied with the number of side points equal to the digital dimension of the spectrum divided by 400, and the resulting spectrum is reduced (window averaged) to 1024 spectral points.

Broadband Tuning and Detection. RF detection diodes are either of the Schottky or of the tunnel type. The latter usually accepts a lower maximum microwave power and is thus easier to be "burned out" by accident, that is with an incorrect power setting by the experimenter. Of relevance here are the broadband characteristics of Schottky diodes (Figure S3). For example, diodes used in X-band bridges can be employed over a wider range than that of the X-band microwave source but typically not below a few GHz. I chose for a zero-bias Crystek Microwave CPDETLS-4000 detector, which has the advantages of proper frequency range of 10−4000 MHz, high maximal input power of 30 dBm, and low cost. Furthermore, its high output voltage avoids the need to operate a video pre-amplifier, and the linear region of its transfer function runs from circa 0 dBm up to at least 20 dBm, which is a practical range to operate the rapid-scan broadband spectrometer, as discussed below. Above 4 GHz, a Pasternack PE8013 zero-bias Schottky diode (10−18,500 MHz) is used with a lower maximal input power of 20 dBm but with excellent linearity over a wide power and frequency range.

The spectrometer tuning procedure is now as follows: with a particular circulator in place, the SPDT switch (Figure 1) is set open to VST detection and the frequency is scanned for a given power, say 0 dBm, over the circulator's range of operation, thus providing a mode pattern of dips (cf Figure S2). The goal now is to find a dip of sufficient depth (i.e., loaded Q) close to the frequency of interest, which however should be tunable to an output power level exiting port 3 of the circulator of the order of 10−20 dBm for proper signal transfer through the low-frequency diode (<4 GHz) or 0−10 dBm through the high-frequency diode (>4 GHz) for an optimal signal-to-noise ratio. A deeper dip typically means a better loaded Q and thus a better detected signal within the boundary condition of the circa 10 dBm from port 3. Parameters to play with are (i) the input power at port 1 by means of tuning the power of the source and optionally adding an amplifier between the source and circulator to boost the 12 dBm maximal output of the VST in order to end up with a final output power at the diode detector that falls within the linear range of the detector; (ii-a) the length of the cable between port 2 of the circulator and the EPR cell where increased length means sharper dips but therefore also lower dip power levels; (ii-b) for frequencies above circa 500 MHz, the setting of the phase shifter; (iii) the output power from port 3 by insertion of an amplifier between port 3 and the detection system. In practice, I found that cable length should vary, in units of 20 m, from 20 m at 500 MHz to 60 m below 100 MHz, that an amplifier between port 3 and the detector should always be present, and that the option of an amplifier between source and port 1 was not required in the present study. Once these conditions have been established, the microwave power and frequency are set to the dip value of the required resonance, the switch is opened to the detector diode, and the spectrum is recorded with proper modulation amplitude and data collection time.

Comparison of Detection Schemes. In my previous work, broadband EPR was recorded as an absorption signal by direct detection in a relatively slowly varying magnetic field (at least 10 s per scan). In the present work, I added field modulation and/or rapid-field scanning, which leads to a total of four different detection schemes:

Method-A: slow-field scanning with direct detection

Method-B: slow-field scanning with field modulation and diode detection

Method-C: rapid-field scanning with direct detection

Method-D: rapid-field scanning with field modulation and diode detection

For a comparison of their relative sensitivities, I took the spectrum of DPPH at circa 155 MHz under normalized conditions of 200 s total data collection time, filtering of raw data with a Savitzky−Golay filter with side points equal to the raw data dimensionality divided by 400, window-averaging to 1024 points, and finally differentiation of directly detected signals.

The results are presented in Figure 4 where it can be seen that under the chosen conditions, the signal is barely detectable with

https://doi.org/10.1021/acs.jpca.1c01217
J. Phys. Chem. A 2021, 125, 3208−3218

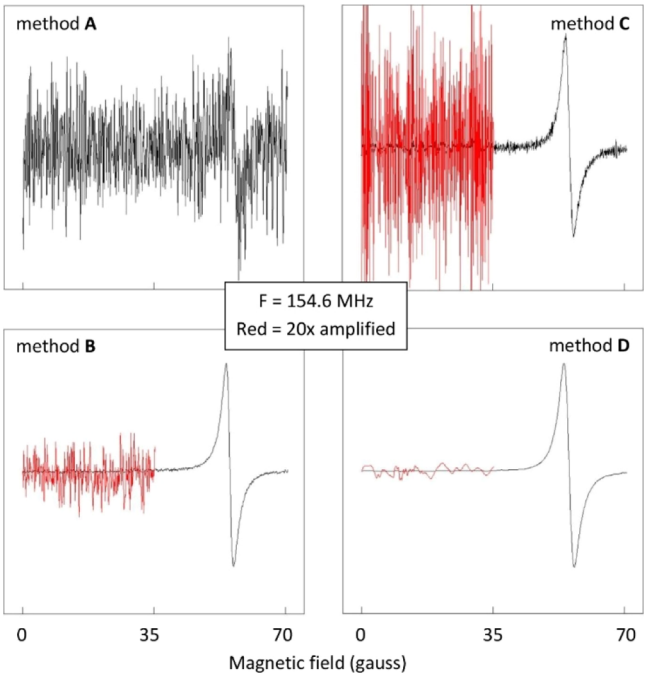

Figure 4. Sensitivity comparison of four detection schemes at low microwave frequency. The methods of slow-field scanning with direct reflected microwave detection (A) or with field modulation (B) and rapid scanning with direct detection (C) or with field modulation (D) were compared for sensitivity in terms of the signal-to-noise ratio of the EPR of a DPPH sample measured under identical conditions: microwave frequency, 154.6 ± 0.2 MHz; elongation cable length, 40 m; dip power, +10 dBm; averaging time, 200 s; and modulation amplitude (if applicable), 0.3 G.

the standard method of direct detection in combination with a slowly scanning field; however, introduction of 100 kHz field modulation with low-frequency diode detection (method-B) leads to an increase in the signal-to-noise ratio by a factor of circa 40, with the restriction that the low-field part of the spectrum is not available due to the finite remnant field of the slowly scanning magnet of circa 37 G. Since rapid-field scanning is only available to frequencies up to some 500−700 MHz, it is clear that method-B is the one of choice for broadband EPR above these frequencies.

When the slowly scanning electromagnet is replaced with the rapidly scanning sets of Helmholtz coils, but without invoking field modulation (method-C), the signal-to-noise ratio is seen to increase by an order of magnitude compared to that of method-A. This approach could be useful for cases in which low-frequency data are of interest, and modulation, for whatever reason, is not desirable.

Finally, when rapid-field scanning is combined with field modulation and diode detection (method-D), the highest signal-to-noise ratio is obtained, although it is only a factor of circa 3 higher than for method-B. This modest increase is presumably due to the fact that the 100 kHz modulation is less efficient when combined with a 100 Hz rapid-field scanning. The sensitivity increase is, however, significant, and the field is available down to 0 G. Furthermore, the noise is of distinctly lower frequency than that seen in the other approaches, indicating that its origin, rather than of purely electronic nature, is perhaps also in the rumble associated with the operation of the Helmholtz coils and/or their cooling and therefore may be amenable to further suppression by improved design. A related performance optimization option would be to fine-tune the modulation frequency to somewhat lower value, although the presently available next value of 10 MHz led to a slightly reduced signal-to-noise ratio, suggesting a significant contribution of flicker noise.

Example: Mono-Heme Low-Spin Fe(III) Cytochrome *c*. To illustrate applicability of the broadband spectrometer to the study of biological systems, I choose examples from the class of low-spin ferric hemes in cytochromes. The paramagnet is $S = 1/2$, and no complications from zero-field interactions can occur. Inhomogeneous broadening at low temperature is completely dominated by *g*-strain, and therefore, the electronic Zeeman interaction and its broadening produce a spectrum that is invariant in the microwave frequency when normalized on an inverse *g*-value scale.[5,6] Thus, the only variations expected with a changing frequency are hyperfine interactions and dipolar interactions. Iron in natural abundance has negligible nuclear spin ($I = 0$ for 98%), so expected hyperfine interactions are limited to ligands to the metal, that is, nitrogens ($I = 1$) and second-sphere protons ($I = 1/2$). Some information on their interaction strength is available from double-resonance experiments, notably electron nuclear double resonance (ENDOR) and electron spin echo envelope modulation (ESEEM) spectroscopy of low-spin ferric hemoproteins.[7−17] Dipolar interaction between the electron spins of hemes has never been explicitly reported; however, the present low-frequency broadband setup should be eminently suitable for its identification. Dipolar interaction can be either intramolecular, for proteins containing more than one heme, or intermolecular between hemes of separate protein molecules, where the latter will be amplified in case the protein tends to dimerize or polymerize in solution.

For a zero-point calibration of the spectroscopy, I picked cytochrome *c* from horse heart because it is a readily available, widely studied, small (12.3 kDa), sturdy protein containing a single heme and with no tendency to polymerize at near neutral pH. On the other hand, it also poses a significant spectroscopic challenge due to its extensive *g* anisotropy ($g \approx 3.06$, 2.23, and 1.20;[5,18] see Figure S4) and pronounced inhomogeneous broadening requiring a field scan up to some 7500 G in X-band for a complete frozen-solution spectrum. For comparison with a more complex system, I chose bacterial (*D. vulgaris* substrain Hildenborough) cytochrome c_3, which is also a small (14 kDa), sturdy protein without tendency to polymerize but containing four hemes per protein molecule. Cytochrome c_3 has been extensively studied in X-band EPR (see below) and has been scrutinized as a paradigm for redox interaction in biological electron transfer.[19]

Using four different spectrometers, we have previously shown that the sharpest feature (the g_z peak) in the spectrum of cytochrome *c* is virtually invariant on a reciprocal *g*-value scale from 35 to 1 GHz.[6] This finding has now been confirmed for the complete spectrum as I find, in an overlay of 9.4 and 1.1 GHz data, only a marginal extra broadening in the low-frequency spectrum (Figure S5). Therefore, our broadband experiment on cytochrome *c* starts at 1.1 GHz; it ends at 233 MHz (Figure 5).

With the frequency being lowered from 1094 to 223 MHz, the spectrum can be seen to be gradually broadening, but even at 233 MHz, the *g* values are clearly resolved. Since cytochrome *c* is a mono-heme protein with no tendency to dimerize, dipolar interactions can only occur between the ferric centers of separate molecules in homogeneous (frozen) solution. A concentration of 5.5 mM means an average Fe−Fe distance of 37.2 Å, as calculated from eq 676 in ref 20, which can be rewritten as

https://doi.org/10.1021/acs.jpca.1c01217
J. Phys. Chem. A 2021, 125, 3208−3218

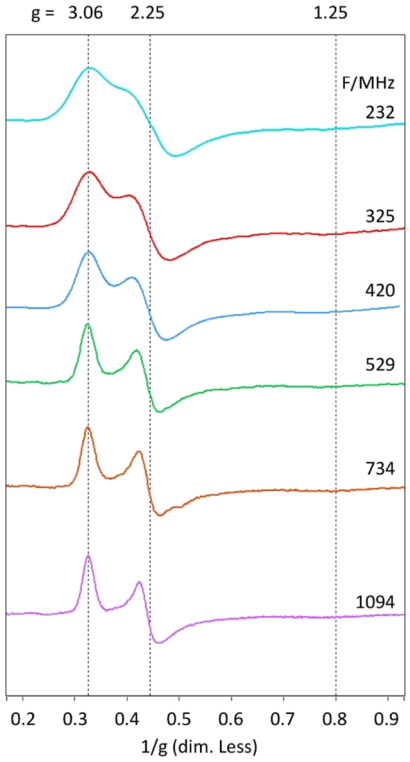

Figure 5. Broadband EPR 2D plot of log(frequency) vs reciprocal g values for cytochrome c from 0.23 to 1.09 GHz. Turning points in the powder pattern are indicated with g values, read-out from the experimental data as peak positions or as zero crossing; they slightly differ from the values in the simulation (cf Figure S5). Spectral zero levels are set to the corresponding log(frequency) value on the y-axis. The sample is 5.5 mM cytochrome c in 100 mM KP_i buffer, pH 7.4. Experimental conditions: the top three spectra were collected in a rapid-field scan (10 ms), the lower three spectra were collected in a slow scan (20 s); dip power, circa +15 dBm; modulation amplitude, 4.8 G or (232 MHz) 3.1 G; elongation cable, 20 m (for 529 MHz and lower); averaging time from top to bottom, respectively, 100, 50, 50, 75, 33, 17 min; temperature, circa 11 K.

$$d = 6.54c^{-1/3}\ \text{Å} \tag{3}$$

in which c is the molar concentration. I have modeled this interaction with the spin Hamiltonian

$$\hat{\mathcal{H}} = \sum_{b=1}^{8}\left\{\beta B(L\cdot g_a\cdot S_a + L\cdot g_b\cdot S_b) + \frac{\mu_0\beta^2}{4\pi r^3}\left[(g_a\cdot S_a)\cdot(g_b\cdot S_b) - \frac{3(\vec{r}\cdot g_a\cdot S_a)(\vec{r}\cdot g_b\cdot S_b)}{r^2}\right]\right\} \tag{4}$$

in which the term in brackets is the well-known classical expression in the point-dipole approximation (i.e., the interacting dipoles are assumed to be infinitesimally small in geometry) and the summation means that a central ferric ion Fe_a is surrounded by eight Fe_b nearest neighbors at the corners of a cube of edge length $(3/4)^{-1/2}$ surrounding the Fe_a, so that r is the distance between two Fe ions, β is the Bohr magneton, B is the external magnetic field, L is a unit vector along B in the g-tensor axes system, g_i is a g tensor, S_i is a spin vector operator, μ_0 is the vacuum permeability, and arrow-headed r is the vector between Fe_a and its neighbor with length r, wherein r is spread according to a stochastic distribution of particles (eq 671 in ref 20; see Figure S6), hence the hat on the Hamiltonian symbol. The distribution is cut off at circa 20 Å for diamagnetic isolation since the shortest distance from the Fe(III) ion to the surface of the cytochrome c molecule is some 10 Å (Figure S7A). These calculations under a point-dipole model indicate that this concentration broadening only becomes significant at a frequency of circa 60 MHz or less (Figure S8) and that its observation at 223 MHz would require an increase in protein concentration well beyond the solubility of cytochrome c.

For reasons that will become clear below, I have also considered the possibility that the point-dipole model would not give a proper description of intermolecular dipole interaction because the ferric dipole might extend considerably over the protoporphyrin IX macrocycle ligand and over the axial amino acid ligands, histidine-18 and methionine-80. To probe the effect of this assumption, I took a simple model in which the dipole is a geometric sphere of given radius around the Fe ion. For a physically reasonable value of $r \approx 5$ Å (Figure S7B), this afforded a broadening at 233 MHz that is significant (Figure S8) and measurable but not extensive enough to explain the full broadening observed experimentally. Therefore, broadening must also involve unresolved SHF interactions from ligand atoms with a nuclear spin.

Candidates for these interactions are specific ^{14}N ($I = 1$) and ^{1}H ($I = 0.5$) atoms (Figure S9), namely, the four tetrapyrrole nitrogen ligands and the ε-nitrogen (and possibly the δ-nitrogen) from the axial ligand histidine-18, and a large number of protons, that is, from the four meso-C's of the tetrapyrrole system, from the α-CH_2 protons on the outer pyrrole substituents, and from the axial ligands, for example, C-2 protons on methionine-80 and C-2 and δ-N protons on His-18. The method of choice to resolve these SHF splittings would be double-resonance spectroscopy, in particular ENDOR and ESEEM. Unfortunately, the literature on this matter is plainly disappointing. The only ENDOR data on cytochrome c is a 1976 preliminary report on observation of nitrogen peaks without interpretation.[7] A single ESEEM study on cytochrome c claims an average hyperfine splitting of 4.4 MHz based on an "approximate fit by simulation", which is impossible to check since no spectral data were provided.[9]

The only other c-type cytochrome studied by proton ENDOR and nitrogen ESEEM is a bacterial c_6 with His and Met axial ligation but otherwise little sequence homology with horse cytochrome c.[15,16] A handful of a-type and b-type heme containing proteins (e.g., myoglobin low-spin derivatives) has been studied by ENDOR or ESEEM,[7−14,17] and from these data together with the sketchy data on the two c-type cytochromes, I deduce the following qualitative picture. The four tetrapyrrole nitrogens and the coordinating His-nitrogen afford a splitting of some 1.6 G with little anisotropy. Protons from C-2 Met and from C2 His and δ-N His give splittings of the order of 1 G possibly with significant anisotropy. The four tetrapyrrole meso-protons give splittings of circa 0.25−0.3 G, and the α-CH_2 protons on the outer pyrrole carbons each contribute a splitting of some 0.15−0.2 G. I took these data as the basis for an approximate model to simulate the low-frequency EPR spectrum of cytochrome c, in which the high-frequency g-stain was extrapolated to low frequency and convoluted with the SHF data. Anisotropy and nitrogen quadrupole interaction were ignored. Simulations show that the observed low-frequency broadening is completely dominated by nitrogen SHF, but that possible resolution of these splittings is blurred away by the proton splittings from the axial amino acid ligands, and other

https://doi.org/10.1021/acs.jpca.1c01217
J. Phys. Chem. A 2021, 125, 3208−3218

proton splittings were too weak to contribute to the CW-EPR broadening. A fit of the 233 MHz spectrum (Figure S10) in which the broadening was taken to be a convolution of *g*-strain, unresolved dipolar interaction and unresolved ligand hyperfine interaction felt significantly short of reproducing the experimentally observed broadening at least when dipolar broadening was assumed to be described by the point-dipole model. When, however, a finite-sphere dipole was assumed, the simulation approached the contours of the experimental spectrum.

Second Example: Tetra-Heme Low-Spin Fe(III) Cytochrome c_3. With the broadband EPR analysis of cytochrome *c* as a calibration marker, I now turn my attention to the more complex system of cytochrome c_3, a protein that packs four hemes in a polypeptide wrap with a volume similar to that of mono-heme cytochrome *c* (Figure S11). Multi-heme proteins have been found to occur quite commonly in nature,[21,22] for example, for the transfer of electrons over longer distances. In addition to this "biological wire" function, they may also exhibit more complex mechanisms of action by means of redox interaction, that is, (anti-) cooperativity in reduction potentials. Cytochrome c_3 is readily obtained in large quantities from sulfate-reducing bacteria and has a longstanding status as paradigmatic redox interaction protein: its single-electron transferring hemes cooperate to form a de facto electron-pair donor/acceptor system for enzymes, such as hydrogenase, that catalyze redox reactions involving two reducing equivalents.[19]

Several groups have studied cytochrome c_3 with conventional X-band EPR spectroscopy,[23−37] and some have tried to deconvolute the complex spectrum in terms of four spectrally independent components.[29,30,32,36] In other words, although redox interaction between the hemes was known to occur, magnetic dipolar interaction was generally, and silently, assumed to be absent. In one case, the dipolar interaction between the heme pair with the smallest interheme distance was simulated in the point-dipole approximation and was found to be insignificant at X-band.[33] We can now more rigorously check the validity of this assumption and also monitor the onset of pairwise interactions as a function of microwave frequency.

To begin with, the EPR as function of decreasing microwave frequency for cytochrome c_3 is very different from that of mono-heme cytochrome *c*, as illustrated in Figure 6.

The details of the X-band spectrum are lost with decreasing frequency to the extent that essentially only a single broad line predominates below some 1 GHz where the spectrum of cytochrome *c* still essentially retains its high-frequency resolution (Figure 5). Clearly, dipolar interactions between the Fe(III) centers prevail, and their nature must be intramolecular, since the protein size is similar to that of cytochrome *c*, and the protein concentration used is significantly lower.

As an aside, it is worth mentioning that during the optimization of the cytochrome c_3, broadband EPR I regularly noticed a contaminating Cu(II) signal that was eventually traced down to ions dissolved from the copper parts of the sample cell. The adventitious signal was eliminated by replacement of the copper ground plate with an aluminum one and replacement of the copper micro wire with a silver one (Figure S12).

I start the analysis with an attempt to simulate the complete X-band spectrum as a sum of four $S = 1/2$ rhombic powder patterns in equimolar concentration. The result is presented in Figure 7.

Broadening by g-strain has been assumed to be colinear, that is, to be defined by three width parameters per individual spectrum. Non-colinearity typically results in asymmetry of the

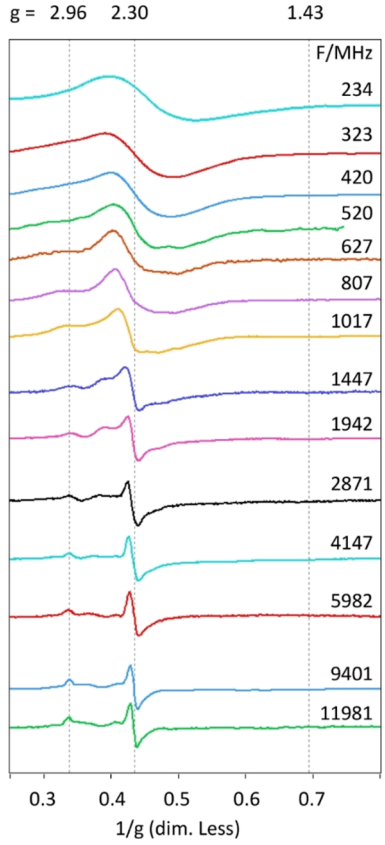

Figure 6. Broadband EPR 2D plot of log(frequency) vs reciprocal *g* values for cytochrome c_3 from 234 to 11981 MHz. Turning points are indicated as effective *g* values for one of the four hemes, namely, the one with presumably the sharpest spectrum in an X-band simulation assuming the absence of dipolar interactions (see Figure 7, below). Spectral zero levels are set to the corresponding log(frequency) value on the *y*-axis. The predicted two waves of dipolar broadening (cf Figure 8) are observed as shifts with frequency changes in the sharp features of the high-frequency, lower half of the figure, and as massive broadening in the low-frequency, top half of the figure. The sample is 1.4 mM *D. vulgaris*, Hildenborough cytochrome c_3 in 100 mM potassium phosphate buffer, pH 7.4. Experimental conditions: the upper four spectra were collected with a rapid-field scan (10 ms) and the rest with a slow scan (20−30 s); the 9401 MHz spectrum was taken with a regular X-band spectrometer (Bruker EMX^{Plus}) in a single 4 min scan; dip power, 10−13 dBm; modulation amplitude, 3.1 G (top four spectra), 4.9−6.1 G, 10 G (X-band), and 16 G (11981 MHz; see Table S2 for details of the microwave configuration); and temperature 10−13 K. The elongation cable was 40 m for the first two spectra and 20 m for the next four spectra. The total data collection time in minutes, from top to bottom, was 60, 20, 20, 20, 33, 30, 15, 33, 10, 33, 17, 60, 4 (X-band), 150. The increasing measuring times at the extreme frequencies indicate the effects of a deteriorating Boltzmann population difference at low frequency and wide field ranges at high frequency. The overall variation in measuring time is related to the use of different circulators and RF amplifiers.

resonance, and this can indeed slightly improve the fit especially in the g_x region; however, it would require the addition of another 12 fitting parameters. The present fit is good enough for our purposes, namely, to draw the conclusion that the spectrum can be approximately, but not exactly, fit as a sum of four low-spin hemes. There is a distinct misfit in the region around circa 2500 G where the shape of the lowest $g_z \approx 2.76$ peak is not faithfully reproduced not even with the inclusion of non-colinear g-strain. I hypothesize that this misfit is a sign of interheme

https://doi.org/10.1021/acs.jpca.1c01217
J. Phys. Chem. A 2021, 125, 3208−3218

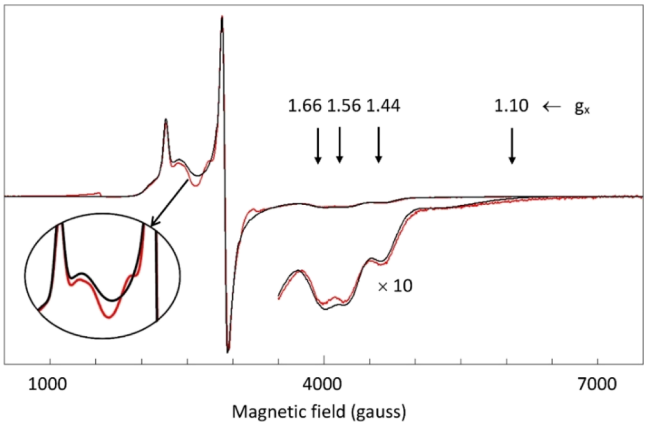

Figure 7. *g*-strain simulation of the X-band spectrum of cytochrome c_3. The sample was the same as shown in Figure 6. The simulation assumes four low-spin hemes in stoichiometric amounts broadened by co-linear *g*-strain but magnetically mutually independent (i.e., absence of dipolar interaction). A reasonable but not perfect simulation is obtained over the whole spectral range. Minor misfits might be due to neglect of non-diagonal *g*-strain elements; however, the misfit in the g_z region (blow up) appears to be real as it is not improved by invoking non co-linear *g*-strain. It is taken as a sign that dipole−dipole interactions cannot be neglected even in X-band. Experimental conditions: microwave frequency, 9400.56 MHz, microwave power, −18 dB of 200 mW; modulation frequency, 100 kHz; modulation amplitude, 10 G; and temperature, 20 K. Simulation parameters, that is, *g* values and *g*-strain line widths, of four ferric hemes: (1) $g_{x,y,z}$ = 1.100, 2.270, 3.150, $\Delta_{xx,yy,zz}$ = 0.125, 0.024, 0.160; (2) $g_{x,y,z}$ = 1.438, 2.300, 2.963, $\Delta_{xx,yy,zz}$ = 0.048, 0.018, 0.042; (3) $g_{x,y,z}$ = 1.555, 2.300, 2.940, $\Delta_{xx,yy,zz}$ = 0.055, 0.018, 0.140; and (4) $g_{x,y,z}$ = 1.665, 2.318, 2.760, $\Delta_{xx,yy,zz}$ = 0.075, 0.018, 0.155.

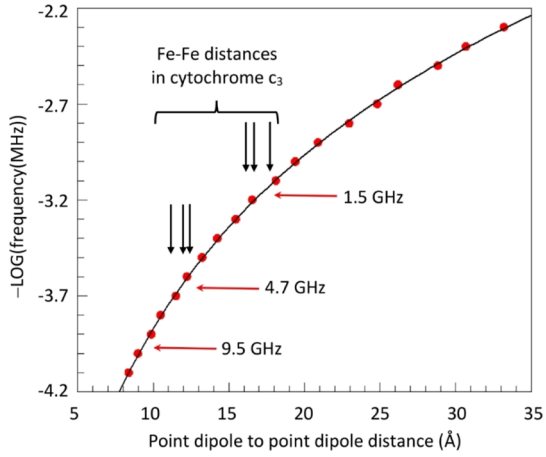

Figure 8. Onset of dipolar broadening with decreasing frequency in tetra-heme cytochrome c_3. The heme with the narrowest line widths from g-strain (component 2, as shown in Figure 7) was taken as an approximative monitor of the very onset of broadening under the point-dipole model by calculating, for a given frequency, at what Fe−Fe distance dipolar broadening with an identical center with co-linear g tensor would cause the sharpest feature (the derivative shape at g_y = 2.300) to be broadened by 20%. The calculated data points follow the $1/r^3$ dependence of dipole−dipole broadening (the black line). The six Fe−Fe distances in cytochrome c_3 are indicated as black vertical arrows. Analysis indicates that broadening should not be observable above some 4.7 GHz and should become dominant well below 1.5 GHz. Since this conclusion is at variance with experimental observation (in particular, see Figure 9, below), I conclude that also for this hemoprotein, now with intramolecular dipolar interaction, the point-dipole assumption for the magnetic dipolar interaction is invalid.

dipolar interactions. Finally, note that for the heme with the largest *g* anisotropy, the lowest $g_x \approx 1.10$ value cannot be read directly from the experimental spectrum; it can only be estimated by simulation.

As a next step, I made an estimate of the earliest possible onset of dipolar interaction as a function of reducing microwave frequency and Fe(III) to Fe(III) distance by taking the sharpest of the four spectra from the X-band simulation and calculating the interaction spectrum in the point-dipole approximation between two hypothetical hemes each with this spectrum and with colinear molecular axis systems. As the criterion for "onset", I took 20% broadening of the sharpest line in the spectrum, that is, the g_y feature. The result is given in Figure 8, and the calculated points obviously follow a trend line for an interaction proportional to $1/r^3$.

Also indicated in the figure are the six Fe−Fe distances (cf Figure S11) taken from the X-ray structure (2cth.pdb) of *D. vulgaris* Hildenborough cytochrome c_3.[38] These distances can be seen to separate into two groups, one covering the approximate range 11−12 Å and the other for 16−18 Å, suggesting that in the broadband EPR one should observe two subsequent "waves" of dipolar interaction becoming manifest at two different frequency ranges. Indeed, one sees in Figure 6, starting from the high-frequency end at the bottom, a changing of apparent line positions in the lower half of the figure, followed by a massive broadening in the upper half. Experimentally, however, the onset of these two waves is found to occur at significantly higher frequency than that predicted in Figure 8.

The unavoidable conclusion appears to be that the point-dipole approximation leads to a severe underestimation of the dipolar interaction strength as a function of the Fe−Fe distance. To work toward the beginning of a solution of this problem, one could perhaps, in analogy to what has been proposed by Bertrand et al. for iron−sulfur clusters with delocalized spin,[39] employ a spin system that is partially delocalized over the porphyrin macrocycle and over the axially coordinating amino acids, as indicated by the SHF splittings reported for hemoproteins on the basis of ENDOR and ESEEM experiments[7−17] and supported by the broadband EPR of mono-heme cytochrome *c* analyzed above. Herewith, however, the problem does become exceedingly complex, the more so, since its quantitative analysis would require, for a four-heme system, repeated diagonalization of a densely filled 16 × 16 interaction matrix. I have not tried to tackle this huge problem in the present context.

Qualitatively, we can draw a few important conclusions. First and foremost it turns out that dipolar interaction can show up in X-band EPR of multi-heme proteins even when simulation on the basis of a point-dipole model would suggest this not to be the case. For an actual illustration of this phenomenon, consider the comparison of low-field details of cytochrome c_3 spectra at some 12, 9, and 6 GHz, as shown in Figure 9A.

It is clear that the main g_z peak that was not properly reproduced in the fit of the X-band spectrum as a sum of four independent hemes, moves with the frequency and thus does not represent a real *g* value. Comparison of the high-field details at these frequencies is hampered by noise caused by the required wide field ranges, but a comparison of the X-band spectrum with one taken at some 4 GHz clearly shows large movements also of g_x peaks (Figure 9B).

It follows as a corollary that *g* values determined from X-band spectral simulations under the assumption of absence of

https://doi.org/10.1021/acs.jpca.1c01217
J. Phys. Chem. A 2021, 125, 3208−3218

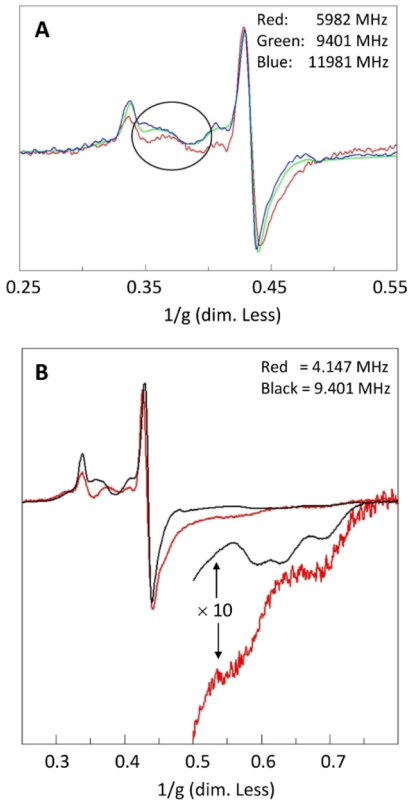

Figure 9. Comparison of the EPR of cytochrome c_3 at different frequencies. The sample is the same as shown in Figure 6. (A) Comparison at 5982.00, 9400.56, and 11,980.80 MHz. The spectrum is not frequency invariant. In particular, a feature that was assigned to a g_z = 2.76 of a non-interacting heme in the simulation, as shown in Figure 7, clearly moves to higher apparent g value with increasing frequency. The observation implies that there is a considerable contribution from dipolar interaction to the X-band spectrum and possibly even at higher frequencies. This conclusion once more attests to the fact that the point-dipole model fails to quantitatively describe dipolar interaction in hemoproteins. (B) Comparison at 4146.61 and 9400.56 MHz. Large shifts in field positions of several spectral features are observed especially of the weak peaks at high field that were attributed to g_x peaks in the simulation of Figure 7 under the assumption of no dipolar interaction. The comparison clearly shows quite strong dipolar interaction to be present at 4.15 GHz, which is at variance with the simple predictions in Figure 8 based on the point-dipole interaction model.

magnetic interactions (Figure 7 and refs 29, 30, 32, 36) are inaccurate insofar as they are shifted by dipolar interactions. In a similar vein, inaccuracy, by neglect of dipolar interactions, may have affected determination of g-tensor axes in single-crystal X-band EPR studies of cytochrome c_3.[31,37] Another implication is that X-band analysis using stepwise chemical reduction of the hemes to diamagnetic low-spin Fe(II) systems[24−30,34] is inaccurate since it will stepwise switch-off pairwise dipolar interactions and thus will change the shape of the individual spectra of the hemes that remain oxidized. Here, a general message could be to take up the challenge of repeating all those experiments at significantly higher microwave frequencies. Also, the massive dipolar broadening that occurs at sub-gigahertz frequencies (cf Figure 6) precludes any possibility to quantitatively study SHF interactions in these systems by cw-EPR spectroscopy.

Finally, in a study on a "basic" form (i.e., overall positively charged at neutral pH) of *Desulfovibrio africanus*, cytochrome c_3 observation suggested an exchange interaction between two of the hemes,[35] although there does not appear to be anything in the crystal structure of this protein to suggest such an interaction.[40] Similar claims have been made for other, eight heme containing proteins.[41,42] Since it is not clear what the physical basis of such an interaction could be, it might be worthwhile to revisit these systems with a new knowledge that intramolecular dipolar interaction between hemes can be significantly more pronounced than expected from prediction on the basis of the point-dipole assumption.

CONCLUSIONS

With the constructed spectrometer, EPR spectra of metalloproteins can be obtained at any frequency over a range of at least some six octaves. For mono-heme ferricytochrome c, a combination of SHF broadening and concentration-dependent intermolecular dipolar interaction gradually adds below 1 GHz to the familiar g-strain. In tetra-heme cytochrome c_3, dipolar effects can already be observed in the X-band, and this puts doubt on the validity of redox interaction studies based on conventional X-band EPR. Massive broadening from multiple pairwise interaction sets in at some 2 GHz and masks any SHF interaction. The onset of dipolar interaction with frequency lowering occurs at higher frequencies than predicted in a point-dipole approach, thus questioning the validity of this model as a descriptor of dipolar interactions between low-spin hemes.

ASSOCIATED CONTENT

Supporting Information

The Supporting Information is available free of charge at https://pubs.acs.org/doi/10.1021/acs.jpca.1c01217.

Spectrometer hardware: detailed part list of the broadband spectrometer, mode pattern for very long resonator circuit, transfer function of RF diode detectors; additional cytochrome EPR data: simulation of cytochrome c X-band EPR, comparison of cytochrome c EPR at 1.1 versus 9.4 GHz, stochastic distance distribution between cytochrome c molecules, cartoon of cytochrome c intermolecular dipolar interaction models, simulated broadening of cytochrome c EPR by dipolar interaction, outline of magnetic nuclei that potentially contribute to SHF interaction with Fe(III) in cytochrome c, simulation of convoluted broadening mechanism that contribute to the very low-frequency EPR of cytochrome c, contaminating signals from resonator-derived copper ions in cytochrome c_3 EPR; and software: programs to simulate the spectrum of a low-spin ferric hemoprotein (here cytochrome c) broadened by (i) g-strain only, (ii) g-strain plus dipolar interaction, and (iii) g-strain plus dipolar interaction plus SHF interaction (PDF)

Complete source code of the spectrum simulation programs (ZIP)

AUTHOR INFORMATION

Corresponding Author

Wilfred R. Hagen − *Department of Biotechnology, Delft University of Technology, 2629HZ Delft, The Netherlands;* orcid.org/0000-0002-1609-6671; Email: W.R.Hagen@tudelft.nl

Complete contact information is available at:

https://pubs.acs.org/10.1021/acs.jpca.1c01217

Notes

The author declares no competing financial interest.

REFERENCES

(1) Hagen, W. R. Broadband tunable electron paramagnetic resonance spectroscopy of dilute metal complexes. *J. Phys. Chem. A* **2019**, *123*, 6986−6995.

(2) Hagen, W. R. *Biomolecular EPR Spectroscopy*; CRC Press, Taylor & Francis Group: Boca Raton, FL, 2009.

(3) Verhagen, M. F. J. M.; Pierik, A. J.; Wolbert, R. B. G.; Mallée, L. F.; Voorhorst, W. G. B.; Hagen, W. R. Axial coordination and reduction potentials of the sixteen hemes in high-molecular mass cytochrome c from Desulfovibrio vulgaris (Hildenborough). *Eur. J. Biochem.* **1994**, *225*, 311−319.

(4) Albracht, S. P. J. A low-cost cooling device for EPR measurements at 35 GHz down to 4.8 °K. *J. Magn. Reson.* **1974**, *13*, 299−303.

(5) Hagen, W. R. Dislocation strain broadening as a source of anisotropic linewidth and asymmetrical lineshape in the electron paramagnetic resonance spectrum of metalloproteins and related systems. *J. Magn. Reson.* **1981**, *44*, 447−469.

(6) Hagen, W. R. g-Strain: Inhomogeneous Broadening in Metalloprotein EPR. CH 22 In *Advanced EPR; Applications in Biology and Biochemistry*; Hoff, A. J., Ed.; Elsevier: Amsterdam, 1989.

(7) Scholes, C. P.; van Camp, H. L. ENDOR from nitrogens and protons in low spin ferric heme and hemoproteins. *Biochim. Biophys. Acta* **1976**, *434*, 290−296.

(8) Mulks, C. F.; Scholes, C. P.; Dickinson, L. C.; Lapidot, A. Electron nuclear double resonance from high- and low-spin ferric hemoglobins and myoglobins. *J. Am. Chem. Soc.* **1979**, *101*, 1645−1654.

(9) Peisach, J.; Mims, W. B.; Davis, J. L. Studies of the electron-nuclear coupling between Fe(III) and ^{14}N in cytochrome P-450 and in a series of low spin heme compounds. *J. Biol. Chem.* **1979**, *254*, 12379−12389.

(10) Martin, C. T.; Scholes, C. P.; Chan, S. I. The identification of histidine ligands to cytochrome a in cytochrome c oxidase. *J. Biol. Chem.* **1985**, *260*, 2857−2861.

(11) Scholes, C. P.; Falkowski, K. M.; Chen, S.; Bank, J. Electron nuclear double resonance (ENDOR) of bis(imidazole)-ligated low-spin ferric heme systems. *J. Am. Chem. Soc.* **1986**, *108*, 1660−1671.

(12) Magliozzo, R. S.; Peisach, J. Electron spin echo envelope modulation spectroscopy of iron-nitrogen interactions in myoglobin hydroxide and Fe(III) tetraphenylporphyrin models. *Biochemistry* **1992**, *31*, 189−199.

(13) Magliozzo, R. S.; Peisach, J. Evaluation of nitrogen nuclear hyperfine and quadrupole coupling parameters for the proximal imidazole in myoglobin-azide, -cyanide, and −mercaptoethanol complexes by electron spin echo envelope modulation spectroscopy. *Biochemistry* **1993**, *32*, 8446−8456.

(14) García-Rubio, I.; Martínez, J. I.; Picorel, R.; Yruela, I.; Alonso, P. J. HYSCORE spectroscopy in the cytochrome b_{559} of the photosystem II reaction center. *J. Am. Chem. Soc.* **2003**, *125*, 15846−15854.

(15) García-Rubio, I.; Medina, M.; Cammack, R.; Alonso, P. J.; Martínez, J. I. CW-EPR and ENDOR studies of cytochrome c_6 from Anabaena PCC 7119. *Biophys. J.* **2006**, *91*, 2250−2263.

(16) García-Rubio, I.; Alonso, P. J.; Medina, M.; Martínez, J. I. Hyperfine correlation spectroscopy and electron spin echo envelope modulation spectroscopy study of the two coexisting forms of the hemoprotein cytochrome c_6 from Anabaena Pcc7119. *Biophys. J.* **2009**, *96*, 141−152.

(17) Van Doorslaer, S.; van den Bosch, M.; Tilleman, L.; Dewilde, S. EPR analysis of imidazole binding to Methanosarcina acetivorans protoglobin. *Appl. Magn. Reson.* **2015**, *46*, 421−433.

(18) Salmeen, I.; Palmer, G. Electron paramagnetic resonance of beef-heart ferricytochrome c. *J. Chem. Phys.* **1968**, *48*, 2049−2052.

(19) Turner, D. L.; Catarino, T. Homotropic and heterotropic interactions in cytochromes c_3 from sulphate reducing bacteria. *FEBS Lett.* **2012**, *586*, 494−503.

(20) Chandrasekhar, S. Stochastic problems in physics and astronomy. *Rev. Mod. Phys.* **1943**, *15*, 1−89.

(21) Bewley, K. D.; Ellis, K. E.; Firer-Sherwood, M. A.; Elliott, S. J. Multi-heme proteins: nature's electronic multi-purpose tool. *Biochim. Biophys. Acta* **2013**, *1827*, 938−948.

(22) Edwards, M. J.; Richardson, D. J.; Paquete, C. M.; Clarke, T. A. Role of multiheme cytochromes involved in extracellular anaerobic respiration in bacteria. *Protein Sci.* **2019**, *29*, 830−842.

(23) Devartanian, D. V.; Legall, J. Electron paramagnetic resonance studies on the reaction of exogenous ligands with cytochrome c_3 from Desulfovibrio vulgaris. *Biochim. Biophys. Acta* **1971**, *243*, 53−65.

(24) Dervartanian, D. V.; Xavier, A. V.; Le Gall, J. EPR determination of the oxidation-reduction potentials of the hemes in cytochrome c_3 from Desulfovibrio vulgaris. *Biochimie* **1978**, *60*, 321−325.

(25) Xavier, A. V.; Moura, J. J. G.; Legall, J.; Dervartanian, D. V. Oxidation-reduction potentials of the hemes in cytochrome c_3 from Desulfovibrio gigas in the presence and absence of ferredoxin by EPR spectroscopy. *Biochimie* **1979**, *61*, 689−695.

(26) Gayda, J.-P.; Bertrand, P.; More, C.; Guerlesquin, F.; Bruschi, M. EPR potentiometric titrations of c_3-type cytochromes. *Biochim. Biophys. Acta* **1985**, *829*, 262−267.

(27) Gayda, J. P.; Yagi, T.; Benosman, H.; Bertrand, P. EPR redox study of cytochrome c_3 from Desulfovibrio vulgaris Miyazaki. *FEBS Lett.* **1987**, *217*, 57−61.

(28) Moura, I.; Teixeira, M.; Huynh, B. H.; LeGall, J.; Moura, J. J. G. Assignment of individual heme EPR signals of Desulfovibrio baculatus (strain 9974) tetraheme cytochrome c_3; A redox equilibria study. *Eur. J. Biochem.* **1988**, *176*, 365−369.

(29) Gayda, J.-P.; Benosman, H.; Bertrand, P.; More, C.; Asso, M. EPR determination of interaction redox potentials in a multiheme cytochrome: cytochrome c_3 from Desulfovibrio desulfuricans Norway. *Eur. J. Biochem.* **1988**, *177*, 199−206.

(30) Benosman, H.; Asso, M.; Bertrand, P.; Yagi, T.; Gayda, J.-P. EPR study of the redox interactions in cytochrome c_3 from Desulfovibrio vulgaris Miyazaki. *Eur. J. Biochem.* **1989**, *182*, 51−55.

(31) Guigliarelli, B.; Bertrand, P.; More, C.; Haser, R.; Gayda, J. P. Single-crystal electron paramagnetic resonance study of cytochrome c_3 from Desulfovibrio desulfuricans Norway strain; Assignment of the heme midpoint redox potentials. *J. Mol. Biol.* **1990**, *216*, 161−166.

(32) More, C.; Gayda, J. P.; Bertrand, P. Simulations of the g-strain broadening of low-spin hemoprotein EPR spectra based on the t_{2g} hole model. *J. Magn. Reson.* **1990**, *90*, 486−499.

(33) Bertrand, P.; Asso, M.; Mbarki, O.; Camensuli, P.; More, C.; Guigliarelli, B. Individual redox characteristics and kinetic properties of the hemes in cytochromes c_3: New methods of investigation. *Biochimie* **1994**, *76*, 524−536.

(34) Morais, J.; Palma, P. N.; Frazão, C.; Caldeira, J.; LeGall, J.; Moura, I.; Moura, J. J. G.; Carrondo, M. A. Structure of the tetraheme cytochrome from Desulfovibrio desulfuricans ATCC 27774: X-ray diffraction and electron paramagnetic resonance studies. *Biochemistry* **1995**, *34*, 12830−12841.

(35) Magro, V.; Pieulle, L.; Forget, N.; Guigliarelli, B.; Petillot, Y.; Hatchikian, E. C. Further characterization of the two tetraheme cytochromes c_3 from Desulfovibrio africanus; nucleotide sequences, EPR spectroscopy and biological activity. *Biochim. Biophys. Acta* **1997**, *1342*, 149−163.

(36) Einsle, O.; Foerster, S.; Mann, K.; Fritz, G.; Messerschmidt, A.; Kroneck, P. M. H. Spectroscopic investigation and determination of reactivity and structure of the tetraheme cytochrome c_3 from Desulfovibrio desulfuricans Essex 6. *Eur. J. Biochem.* **2001**, *268*, 3028−3035.

(37) Saitoh, T.; Tachibana, Y.; Higuchi, Y.; Hori, H.; Akutsu, H. Correlation between the g tensors and the nonplanarity of porphyrin rings in Desulfovibrio vulgaris Miyazaki F cytochrome c_3, studied by single crystal EPR. *Bull. Chem. Soc. Jpn.* **2004**, *77*, 357−363.

(38) Simões, P.; Matias, P. M.; Morais, J.; Wilson, K.; Dauter, Z.; Carrondo, M. A. Refinement of the three-dimensional structures of cytochrome c_3 from Desulfovibrio vulgaris Hildenborough at 1.67 Å

resolution and from Desulfovibrio desulfuricans ATCC 27774 at 1.6 Å resolution. *Inorg. Chim. Acta* **1998**, *273*, 213−224.
(39) Bertrand, P.; More, C.; Guigliarelli, B.; Fournel, A.; Bennett, B.; Howes, B. Biological polynuclear clusters coupled by magnetic interactions: from the point dipole approximation to a local spin model. *J. Am. Chem. Soc.* **1994**, *116*, 3078−3086.
(40) Pieulle, L.; Morelli, X.; Gallice, P.; Lojou, E.; Barbier, P.; Czjzek, M.; Bianco, P.; Guerlesquin, F.; Hatchikian, E. C. The type I/type II cytochrome c_3 complex: an electron transfer link in the hydrogen-sulfate reduction pathway. *J. Mol. Biol.* **2005**, *354*, 73−90.
(41) Hendrich, M. P.; Petasis, D.; Arciero, D. M.; Hooper, A. B. Correlations of structure and electronic properties from EPR spectroscopy of hydroxylamine oxidoreductase. *J. Am. Chem. Soc.* **2001**, *123*, 2997−3005.
(42) Maalcke, W. J.; Reimann, J.; de Vries, S.; Butt, J. N.; Dietl, A.; Kip, N.; Mersdorf, U.; Barends, T. R. M.; Jetten, M. S. M.; Keltjens, J. T.; Kartal, B. Characterization of anammox hydrazine dehydrogenase, a key N_2-producing enzyme in the global nitrogen cycle. *J. Biol. Chem.* **2016**, *291*, 17077−17092.

https://doi.org/10.1021/acs.jpca.1c01217
J. Phys. Chem. A 2021, 125, 3208−3218